



Review

The developments and challenges of cerium half-cell in zinc–cerium redox flow battery for energy storage

Zhipeng Xie^{a,b}, Qingchao Liu^a, Zhiwen Chang^a, Xinbo Zhang^{a,*}

^a State Key Laboratory of Rare Earth Resource Utilization, Changchun Institute of Applied Chemistry, Chinese Academy of Sciences, Changchun 130022, PR China

^b College of Chemistry and Chemical Engineering, Jiangxi University of Science and Technology, Ganzhou 341000, PR China

ARTICLE INFO

Article history:

Received 10 September 2012

Received in revised form

13 December 2012

Accepted 14 December 2012

Available online 25 December 2012

Keywords:

Energy storage

Zinc–cerium redox flow batteries

Rare earths

Electrolyte

Catalyst

ABSTRACT

Zinc–cerium redox flow batteries (ZCBs) are emerging as a very promising new technology with the potential to store a large amount of energy economically and efficiently, thanks to its highest thermodynamic open-circuit cell voltage among all the currently studied aqueous redox flow batteries. However, there are numerous scientific and technical challenges that must be overcome if this alluring promise is to turn into reality, from designing the battery structure, to optimizing the electrolyte compositions and elucidating the complex chemical reactions that occur during charge and discharge. This review article is the first summary of the most significant developments and challenges of cerium half-cell and the current understanding of their chemistry. We are certain that this review will be of great interest to audience over a broad range, especially in fields of energy storage, electrochemistry, and chemical engineering.

© 2012 Elsevier Ltd. All rights reserved.

Contents

| | |
|-------------------------------------|-----|
| 1. Introduction..... | 695 |
| 2. Developments and challenges..... | 696 |
| 2.1. Electrolyte..... | 696 |
| 2.1.1. Single acid medium..... | 696 |
| 2.1.2. Mixed acid media..... | 698 |
| 2.1.3. Additives..... | 699 |
| 2.1.4. Mixed electrolyte..... | 700 |
| 2.2. Electrode..... | 700 |
| 3. Reaction mechanism..... | 702 |
| 4. Conclusions and perspective..... | 702 |
| Acknowledgements..... | 702 |
| References..... | 703 |

1. Introduction

The environmental concerns over the use of fossil fuels and their resource constraints, combined with energy security concerns, have spurred great interest in generating electric energy from renewable sources. Among them, solar [1] and wind [2,3] energies are among the most abundant and potentially readily available. Capturing a small percentage of potential solar and wind energies could contribute significantly to meeting the world's

electrical energy requirements. While advances in technology are still needed to harvest renewable energy economically, solar and wind power technologies have grown quickly. However, solar and wind are not constant and reliable sources of power. The variable nature of these renewable sources causes significant challenges for the electric grid operators because other power plants (usually fossil fueled power plants) need to compensate for the variability. A further concern is the fact that the renewable resources are localized and are often away from load centers. To this end, thanks to its high energy density, simplicity and reliability, electrochemical energy storage (EES) [4,5] has become an issue of strategic importance as it will play a critical role in clean energy generation and use.

* Corresponding author. Tel.: +86 431 85262235.

E-mail address: xbzhang@ciac.jl.cn (X. Zhang).

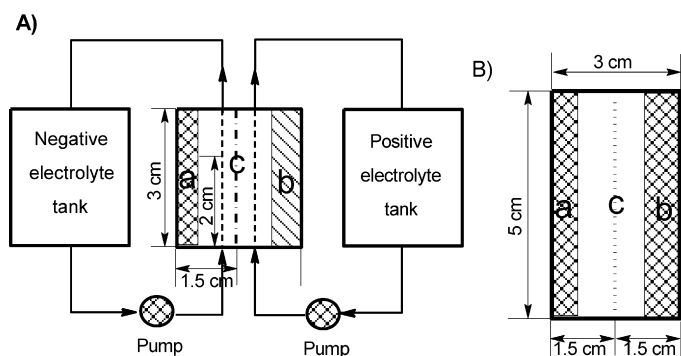


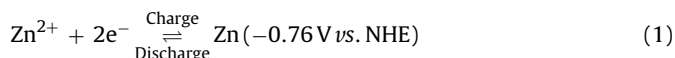
Fig. 1. (A) Front view of the unit Zn/Ce redox flow cell. (B) Vertical view of the unit Zn/Ce redox flow cell. (a) Zinc negative electrode. (b) Carbon felt positive electrode. (c) Nafion 115 ion-exchange membrane. Volume of each tank, 25 mL; flow rate, 11.5 cm min⁻¹.

Redox flow battery (RFB) energy storage systems [6–8] use two soluble redox couple as electroactive species that are oxidized or reduced to store or deliver energy. In the divided mode [9], the electrodes are separated by an ion exchange membrane while the reactants contained in separate storage tanks are recirculated through the redox flow battery where the electrochemical reactions (reduction and oxidation) take place. There are various types of redox flow batteries, such as bromine/polysulphide [10], all vanadium [11–19], zinc/bromine [20–24], zinc/ cerium [25–29] and soluble lead-acid [30–35], all vanadium-acac (acac, acetylacetonate) [36], all chromium-EDTA (EDTA, ethylenediaminetetraacetic acid) [37], all chromium-acac [38], all manganese-acac [39], all ferrum-bpy (bpy, bipyridine) [40], all ruthenium-acac [40], vanadium/bromine [41], ferrum/bromine [42], chromium/ferrum [43,44], vanadium/cerium [45], lead/tiron [46], zinc/nitroso [47], cadmium/chloranil [48], Cu/PbO₂ [49] batteries, which are in the different stage of development. Compared to other electrochemical storage batteries [50–80], electrically rechargeable redox flow systems hold many advantages, including long cycle life, high overall energy efficiency, capability of deep discharge, and especially, the power and energy capacity of the system can be separated – the power of the system is determined by the number of cells in the stack and the size of the electrodes whereas the energy storage capacity is determined by the concentration and volume of the electrolyte. Both energy and power can be easily varied from 10 kWh/10 W to 100 MWh/10 kW.

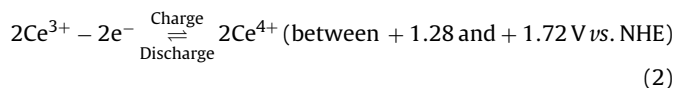
Among all the proposed aqueous RFB systems, zinc–cerium redox flow battery (ZCB) [81–86], consisting of Zn/Zn²⁺ and Ce³⁺/Ce⁴⁺ redox couples, holds the highest theoretical cell voltage (ca. 2.50 V). The standard cell voltage of all-vanadium redox flow battery is only 1.26 V. The higher cell capacity and power can result from a higher cell voltage under a certain concentration of electrolyte. In methanesulfonic acid (MSA) media, the formal Ce³⁺/Ce⁴⁺ potentials vary from the lowest value 1.543 V vs. NHE in 5 mol L⁻¹ MSA at 293 K to 1.629 V vs. NHE in 1 mol L⁻¹ MSA at 313 K ([Ce³⁺] = [Ce⁴⁺] = 0.002 mol L⁻¹). [81] As shown in Fig. 1, similar to other RFB systems, ZCB are based on the combination of two electrochemical half-cells (the negative half-cell and the positive half-cell). In detail, negative zinc electrolyte and positive cerium electrolyte are stored in two separated reservoirs and are circulated during the operation. Negative and positive electrolyte compartments are separated by a membrane (denoted as the separator) and arranged in a “bipolar” cell stack of alternating negative and positive half-cells.

The fundamental battery chemistry [87] during charge/discharge inside the ZCB is as follows:

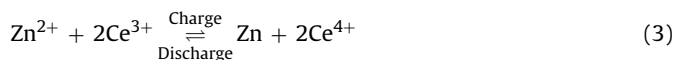
Anode



Cathode



Cell:



In this review article, Section 2, the bulk of the article, summarizes the current developments and main limiting factors of the cerium half-cell. Section 3 introduces the current understanding of its chemistry. Section 4 concludes the information provided in this article and describes the key areas for future research from the perspective of the authors.

2. Developments and challenges

Since ZCB is first proposed by Clarke and co-workers in 2004 [88,89], the electrochemical properties and the characterization of ZCB have been identified. During charge/discharge cycles at 50 mA cm⁻², the coulombic and voltage efficiencies of the zinc–cerium redox flow battery are reported to be 92 and 68%, respectively [83]. Very recently, a membraneless (undivided) zinc–cerium system based on low acid concentration electrolyte using compressed pieces of carbon felt positive electrode is proposed, and the discharge cell voltage and energy efficiency are reported to be approximately 2.1 V and 75%, respectively. With such undivided configuration (single electrolyte compartment), self-discharge is relatively slow at low concentrations of cerium and acid [90].

Although significant improvements have been achieved, ZCB is still in the primary development stage and there are numerous scientific and technical challenges that must be overcome if this alluring promise is to turn into reality. We will summarize the developments and the most significant limiting factors of cerium half-cell, from optimizing their electrolyte compositions, to investigating the electrode.

2.1. Electrolyte

The electrochemical reaction active material of cerium half-cell is dissolved in the electrolyte supporting medium, so the electrolyte is the electric energy carrier and its performance play a crucial role on the performance of ZCB. For example, the solubility of active material is highly supporting medium dependent, which would significantly affect the special power and the energy conversion efficiency of a ZCB. To date, most of the studies about electrolyte are focused on the positive side of ZCB, including single acid medium, mixed acid media, additives, and mixed electrolyte.

2.1.1. Single acid medium

The kinetics of the Ce³⁺/Ce⁴⁺ in single acid media such as sulfuric acid [91–95,96–105], nitric acid [105–108], perchloric acid [91,92,102], methanesulfonic acid [81–83,102] and sulfamic acid [84], as well as the solubility (or stability) [81,86] of the Ce³⁺/Ce⁴⁺ electrolyte in different single acid media, are investigated. Table 1 illustrates the kinetic parameters of the Ce³⁺/Ce⁴⁺ couple in various acid media. It can be clearly found that the kinetics of Ce³⁺/Ce⁴⁺ electrode process are quite different in different supporting media. For example, the standard rate constant varied from 5.0 × 10⁻⁵ cm s⁻¹ in 1 mol L⁻¹ NH₂SO₃H [84] to 2.0 × 10⁻³ cm s⁻¹

Table 1
Kinetic parameters of the Ce³⁺/Ce⁴⁺ redox reaction in different single acid media at platinum electrode.

| Supporting medium | H ₂ SO ₄ [100] | CH ₃ SO ₃ H [81] | HNO ₃ [105] | NH ₂ SO ₃ H [84] |
|--|--------------------------------------|--|------------------------|--|
| Exchange current density $j_0/10^3 \text{ A cm}^{-2}$ | – | 1.32 | – | 0.60 |
| Standard rate constant $k_0/10^4 \text{ cm s}^{-1}$ | 2.96 | 0.55 | 20 | 0.50 |
| Cathodic transfer coefficient/ α | 0.155 | – | – | – |
| Anodic transfer coefficient/ β | 0.197 | – | – | – |
| Ce ³⁺ Diffusion coefficient/ $10^6 \text{ cm}^2 \text{ s}^{-1}$ | – | 5.37 | 8.8 | 5.93 |

in 1 mol L⁻¹ HNO₃ [105] medium. The diffusion coefficient of Ce³⁺ changed from $5.37 \times 10^{-6} \text{ cm}^2 \text{ s}^{-1}$ in 2 mol L⁻¹ CH₃SO₃H [81] to $8.8 \times 10^{-6} \text{ cm}^2 \text{ s}^{-1}$ in 1 mol L⁻¹ HNO₃ [105]. Leung et al. [82] reported a different value, $5.0 \times 10^{-7} \text{ cm}^2 \text{ s}^{-1}$, of Ce³⁺ diffusion coefficient in CH₃SO₃H media. The difference of Ce³⁺ diffusion coefficient between the two literatures [81,82] partly resulted from the different concentrations of Ce³⁺ and CH₃SO₃H in the electrolyte. In addition, the kinetics of the Ce³⁺/Ce⁴⁺ electrode process is significantly affected by the acid medium concentration. In sulfuric acid [103] medium, the peak potential separation changed from 400 mV in 4 mol L⁻¹ H₂SO₄ to almost 1200 mV in 1 mol L⁻¹ H₂SO₄ at 293 K. In methanesulfonic acid [81] medium, the peak potential separation for the redox reactions decreases from 207 to 141 mV with the increase of CH₃SO₃H concentration from 1 to 3 mol L⁻¹. The larger peak splittings indicate a more sluggish interfacial electron transfer process. Wei et al. [105] proposed that high proton concentration promotes the electron transfer of the Ce³⁺/Ce⁴⁺ couple, which is probably because the activated complex can be involved in a protonation or deprotonation equilibrium. As shown in Table 2 [105], the standard rate constant of Ce³⁺/Ce⁴⁺ electrode reaction changed from 4.0×10^{-3} to $2.6 \times 10^{-2} \text{ cm s}^{-1}$ with the increase of proton concentration from 1 to 6 mol L⁻¹. It is worthy noting that the NO₃⁻ ion possibly has a positive effect on the kinetics of the Ce³⁺/Ce⁴⁺ charge transfer process, which is supported by the fact that the standard rate constant of the Ce³⁺/Ce⁴⁺ couple is $4.0 \times 10^{-3} \text{ cm s}^{-1}$ in a solution containing 1 mol L⁻¹ HNO₃ and 5 mol L⁻¹ NaNO₃, whereas it is $2.0 \times 10^{-3} \text{ cm s}^{-1}$ in a solution containing only 1 mol L⁻¹ HNO₃. Generally, the diffusion coefficient of the Ce³⁺/Ce⁴⁺ decreases with the increase of supporting medium concentration. For example, the diffusion coefficient of Ce³⁺ ion is $8.8 \times 10^{-6} \text{ cm}^2 \text{ s}^{-1}$ in 1 mol L⁻¹ HNO₃ solution whereas it is $6.9 \times 10^{-6} \text{ cm}^2 \text{ s}^{-1}$ in 6 mol L⁻¹ HNO₃ solution and $5.5 \times 10^{-6} \text{ cm}^2 \text{ s}^{-1}$ in a solution containing 1 mol L⁻¹ HNO₃ and 5 mol L⁻¹ NaNO₃. With the increase of nitrate ion concentration, there are more large-size electroactive species (e.g., [Ce(NO₃)₂]⁺) in the solution, leading to the increase of diffusion resistance.

The temperature also significantly affects the kinetics of the Ce³⁺/Ce⁴⁺ electrode reaction. For example, in a 6 mol L⁻¹ HNO₃ [105] solution, the standard rate constant of the Ce³⁺/Ce⁴⁺ couple is $2.6 \times 10^{-2} \text{ cm s}^{-1}$ at 298 K whereas it is $4.6 \times 10^{-2} \text{ cm s}^{-1}$ at 333 K (Table 3). The diffusion coefficient of Ce³⁺ ion changes from 6.9×10^{-6} to $1.31 \times 10^{-5} \text{ cm}^2 \text{ s}^{-1}$ when temperature increases from 298 to 333 K. In 2 mol L⁻¹ CH₃SO₃H [81], the peak potential separation of the Ce³⁺/Ce⁴⁺ couple decreases from 203 to 151 mV

Table 2
Kinetic parameters for the Ce³⁺/Ce⁴⁺ couple in nitrate solutions [105].

| HNO ₃ + NaNO ₃ (mol L ⁻¹) | Ce ³⁺ Diffusion coefficient (10 ⁶ cm ² s ⁻¹) | Standard rate constant (10 ⁴ cm s ⁻¹) |
|--|--|---|
| 1+5 | 5.5 | 40 |
| 3+3 | 6.2 | 110 |
| 5+1 | 6.8 | 230 |
| 6+0 | 6.9 | 260 |
| 1+0 | 8.8 | 20 |
| 1+1 | 8.7 | 30 |
| 1+3 | 7.3 | 30 |

when the temperature ranging from 293 to 333 K; meanwhile, anodic peak current increases from 5.559 to 8.080 mA, cathodic peak current increases from 4.963 to 7.059 mA. In 1 mol L⁻¹ H₂SO₄ [45] solution, the anodic and cathodic peak currents increase from 1.05 to 1.98 mA and from 0.47 to 0.89 mA, respectively; while the peak potentials separation decreases from 261 to 148 mV. The increase of peak current is mainly caused by the increase of diffusion coefficient, while the decrease of peak potential separation mainly by the decrease of the Ce³⁺/Ce⁴⁺ charge transfer resistance.

The solubility of cerium salt is quite different in different single acid medium. Generally, in HNO₃ [108], CH₃SO₃H [81,86], and CF₃SO₃H media, cerium salt holds good solubility, while the solubility of cerium salts in sulfuric acid [103] media is relatively low. We have studied the stability of Ce³⁺/Ce⁴⁺ electrolyte in methanesulfonic acid medium [81,86]. The solubility of Ce(CH₃SO₃)₃ is found to decrease continuously with increasing methanesulfonic acid concentration. For example, the solubility of Ce(CH₃SO₃)₃ changed from 2.230 to 1.123 mol L⁻¹ as the methanesulfonic acid concentration ranged from 1 to 3 mol L⁻¹ at 293 K. Higher methanesulfonic acid concentration favors the precipitation of Ce³⁺ ions, but stabilizes Ce⁴⁺ ions. After 12 days, precipitation can be found in a solution containing 1 mol L⁻¹ Ce(CH₃SO₃)₄ and 1 mol L⁻¹ CH₃SO₃H, whereas no precipitate appeared in a solution containing 1 mol L⁻¹ Ce(CH₃SO₃)₄ and 3 mol L⁻¹ CH₃SO₃H even after 30 days at 333 K (Table 4). The rate of thermal precipitation increases with increasing temperature but decreases with increasing acid concentration. At elevated temperatures for extended periods, Ce⁴⁺ can slowly precipitate from solution, the extent and rate of which being dependent on cerium and methanesulfonic acid concentrations, temperature as well as state of charge.

The solubility of cerium sulfates in 0.1–4.0 mol L⁻¹ H₂SO₄ at 293–333 K is investigated by Paulenova [103]. As shown in Table 5, the solubility of both ceric and cerous sulfates decreases continuously with rising sulfuric acid concentration. It can be explained by the well known “common ion effect”. According to “common ion effect”, increase of SO₄²⁻ ion concentration will lead to the decrease of the solubility of both cerium sulfates. At sulfuric acid concentrations less than 2 mol L⁻¹, the effect of temperature on the solubility of both sulfates is most significant, and is almost negligible in 4–6 mol L⁻¹ H₂SO₄. For example, in 1 mol L⁻¹ H₂SO₄ medium, the solubility of Ce₂(SO₄)₃ decreases from 0.151 to 0.068 mol L⁻¹ with temperature ranged from 293 to 333 K; that of Ce(SO₄)₂ decreases from 0.426 to 0.232 mol L⁻¹. However, in 4 mol L⁻¹ H₂SO₄ medium, the solubility difference of cerium sulfates is only 5 mmol L⁻¹ as temperature increases from 293 to 333 K. Increase of temperature would result in a decrease in cerous sulfate solubility, indicating that the dissolution of cerous sulfate is exothermic reaction. The

Table 3
Kinetic parameters of the Ce³⁺/Ce⁴⁺ couple in 6 mol L⁻¹ HNO₃ at various temperatures [105].

| Temperature (K) | Diffusion coefficient (10 ⁶ cm ² s ⁻¹) | Standard rate constant (10 ⁴ cm s ⁻¹) |
|-----------------|---|---|
| 298 | 6.9 | 260 |
| 313 | 9.2 | 370 |
| 333 | 13.1 | 460 |

Table 4
Stability of cerium salts in methanesulfonic acid for 30 days.

| CH ₃ SO ₃ H + Ce(CH ₃ SO ₃) ₃ (mol L ⁻¹) | Temperature (K) | State of charge (%) | | | | | |
|--|-----------------|---------------------|-----|-----|-----|-----|-----|
| | | 0 | 50 | 70 | 80 | 90 | 100 |
| 3+1 | 293 | NPT | NPT | NPT | NPT | NPT | NPT |
| 3+1 | 313 | NPT | NPT | NPT | NPT | NPT | NPT |
| 3+1 | 333 | NPT | NPT | NPT | NPT | NPT | NPT |
| 1+1 | 293 | NPT | NPT | NPT | NPT | NPT | NPT |
| 1+1 | 313 | NPT | NPT | NPT | NPT | NPT | NPT |
| 1+1 | 333 | NPT | NPT | NPT | NPT | NPT | 12d |
| 1+2 | 293 | NPT | NPT | – | – | – | – |
| 1+2 | 313 | NPT | NPT | – | – | – | – |
| 1+2 | 333 | NPT | 18d | – | – | – | – |

Note. NPT means no precipitation.

Table 5
Concentrations of cerium in saturated solutions of Ce₂(SO₄)₃ and Ce(SO₄)₂ in sulfuric acid medium.

| H ₂ SO ₄ (mol L ⁻¹) | Ce ³⁺ /10 ³ (mol L ⁻¹) | | | Ce ⁴⁺ /10 ³ (mol L ⁻¹) | | |
|---|--|-------|-------|--|-------|-------|
| | 293 K | 313 K | 333 K | 293 K | 313 K | 333 K |
| 0 | – | – | – | 703 | 962 | 299 |
| 0.1 | 207 | 122 | 85 | 757 | 910 | 238 |
| 0.5 | – | – | – | – | 629 | – |
| 1 | 151 | 97 | 68 | 426 | 421 | 232 |
| 2 | 89 | 80 | 52 | 276 | 264 | 277 |
| 3 | – | – | – | 155 | 154 | 167 |
| 4 | 20 | 19 | 15 | 76 | 76 | 81 |
| 6 | – | – | – | 25 | 27 | 32 |

complex temperature dependence of the Ce(SO₄)₂ solubility with maximum at 313 K possibly results from hydroxysulfate complexation reaction that resulted in a different reaction enthalpy of dissolution. The exothermic reaction of dissolving of Ce(SO₄)₂ in water is investigated by Jones and Soper [109], who suggested that ceric sulfate exists either as the complex sulfatoceric acid, H₄Ce(SO₄)₄, or as the product of the hydrolysis of this acid, H₄[CeO_x(SO₄)_{4-x}].

2.1.2. Mixed acid media

To further improve the stability of electrolyte with high concentration active material and the kinetics of half-cell reaction, and reduce the cost of ZCB, mixed acid media is proposed to meet these challenges.

We systematically investigated the electrochemical behavior of the Ce³⁺/Ce⁴⁺ couple in mixed acid media containing CH₃SO₃H and H₂SO₄, the stability of electrolyte, as well as performance of Zn/Ce redox flow battery [85]. It is found that the Ce³⁺/Ce⁴⁺ electrode reaction is more reversible in mixed-acid supporting electrolyte. As shown in Table 6, the peak potential separation of the Ce³⁺/Ce⁴⁺ couple are no less than 462 mV in sulfuric acid [100] medium with concentrations no more than 2 mol L⁻¹, and it is 141 mV in 3 mol L⁻¹ CH₃SO₃H [81]. However, the peak potential separation is only 103 mV in a mixed acid [85] media containing 1 mol L⁻¹ CH₃SO₃H and 1 mol L⁻¹ H₂SO₄. Compared with single acid medium, the mixed-acid media have their special advantages. As illustrated

Table 6
Peak potential separations of the Ce³⁺/Ce⁴⁺ couple on platinum electrode at 50 mV s⁻¹.

| Supporting media | ΔE _p (mV) |
|--|----------------------|
| 0.5 mol L ⁻¹ H ₂ SO ₄ | 622 [100] |
| 1.25 mol L ⁻¹ H ₂ SO ₄ | 522 [100] |
| 2 mol L ⁻¹ H ₂ SO ₄ | 462 [100] |
| 1 mol L ⁻¹ CH ₃ SO ₃ H | 207 [81] |
| 2 mol L ⁻¹ CH ₃ SO ₃ H | 157 [81] |
| 3 mol L ⁻¹ CH ₃ SO ₃ H | 141 [81] |
| 1 mol L ⁻¹ CH ₃ SO ₃ H + 1 mol L ⁻¹ H ₂ SO ₄ | 103 [85] |

Table 7
Kinetic parameters for the Ce³⁺/Ce⁴⁺ couple at platinum electrode in mixed acid medium [85].

| CH ₃ SO ₃ H + H ₂ SO ₄ (mol L ⁻¹) | Ce ⁴⁺ Diffusion coefficient (10 ⁶ cm ² s ⁻¹) | Standard rate constant (10 ⁴ cm s ⁻¹) |
|---|---|--|
| 2+0 | 2.56 | 0.79 |
| 2+0.25 | 8.27 | 1.18 |
| 2+0.50 | 6.96 | 1.43 |
| 2+0.75 | 5.87 | 1.48 |

in Table 7, the diffusion coefficient of Ce⁴⁺ ion in mixed acid supporting electrolyte is higher than that in single acid (CH₃SO₃H), which is out of the expectation; and the standard rate constant of the Ce³⁺/Ce⁴⁺ couple in mixed acid media is also higher than that in methanesulfonic acid.

As shown in Table 8, the solubility of cerium salt in mixed acid supporting electrolyte is much higher than that in sulfuric acid. The total SO₄²⁻/HSO₄⁻ concentration can only reach 1.51 mol L⁻¹ before a slight precipitation appears in a 0.5 mol L⁻¹ Ce³⁺ solution without methanesulfonic acid at 298 K. That is to say, the approximate of saturation ion product is 0.86 evaluated from expressions $K_{\text{sip}} = [\text{Ce}^{3+}]^2([\text{SO}_4^{2-}] + [\text{HSO}_4^-])^3$. However, total SO₄²⁻/HSO₄⁻ concentration can reach 2.88 mol L⁻¹ for a 0.5 mol dm⁻³ Ce³⁺ mixed acid solution with 4 mol L⁻¹ CH₃SO₃H. The value of saturation ion product is approximately 5.97, markedly larger than 0.86. The CH₃SO₃H can improve the solubility of Ce₂(SO₄)₃, which is mainly due to the increase of proton concentration. Proton can promote the transformation of SO₄²⁻ into HSO₄⁻, resulting in the decrease of SO₄²⁻ ions and thus allowing the solubility of Ce₂(SO₄)₃ to increase. As shown in Table 9, a 1 mol L⁻¹ Ce mixed-acid solution containing 2 mol L⁻¹ CH₃SO₃H and 0.5 mol L⁻¹ H₂SO₄ at any state of charge is a perfectly stable system at temperatures up to 313 K.

Table 8
The effect of MSA concentration on the saturation ion product of cerous sulphate at 298 K [85].

| MSA (mol L ⁻¹) | Ce ³⁺ (mol L ⁻¹) | Total SO ₄ ²⁻ /HSO ₄ ⁻ (mol L ⁻¹) | | K _{sip} |
|----------------------------|---|---|-------------------|------------------|
| | | No ppt | Slight ppt | |
| 0 | 0.5 | 1.51 ^a | 1.54 ^b | 0.86 |
| 1 | 0.5 | 2.02 ^a | 2.05 ^b | 2.06 |
| 2 | 0.5 | 1.98 ^a | 2.02 ^b | 1.94 |
| 3 | 0.5 | 2.23 ^a | 2.27 ^b | 2.77 |
| 4 | 0.5 | 2.88 ^a | 2.92 ^b | 5.97 |
| 5 | 0.5 | 2.52 ^a | 2.55 ^b | 4.00 |

Note. Total SO₄²⁻ and HSO₄⁻ concentration is calculated according to the amount of sulfuric acid consumed. The values (a) are calculated according to the amount of sulfuric acid consumed before a precipitation emerged (but very close to the saturation state), which had a negative deviation from the saturation value. The values (b) are calculated according to the amount of sulfuric acid consumed until a slight precipitation emerged, which had a positive deviation from the saturation value. The value of saturation ion product (K_{sip}) is calculated according to value (a), so it also had a negative deviation from the true value.

Table 9Stability of 1 mol L⁻¹ cerium in a mixed-acid solution containing 2 mol L⁻¹ CH₃SO₃H and 0.5 mol dm⁻³ H₂SO₄ at different temperatures and states of charge [85].

| Electrolyte | State of charge (%) | Precipitation time (days) | | |
|---|---------------------|---------------------------|-----------------|-----------------|
| | | 293 K | 313 K | 333 K |
| 100%Ce ³⁺ | 0 | No ppt after 30 | No ppt after 30 | No ppt after 30 |
| 30%Ce ³⁺ + 70%Ce ⁴⁺ | 70 | No ppt after 30 | No ppt after 30 | No ppt after 30 |
| 20%Ce ³⁺ + 80%Ce ⁴⁺ | 80 | No ppt after 30 | No ppt after 30 | 18 |
| 10%Ce ³⁺ + 90%Ce ⁴⁺ | 90 | No ppt after 30 | No ppt after 30 | 6 |
| 100%Ce ⁴⁺ | 100 | No ppt after 30 | No ppt after 30 | 3 |

Note. Stability refers to time taken (in days) for a slight precipitate to appear in solution. The mixed acid initially involved 2 mol L⁻¹ CH₃SO₃H and 0.5 mol L⁻¹ H₂SO₄ and is not analyzed after charging.

As illustrated in Fig. 1 [85], the total volume of the cell is 3 cm × 5 cm × 3 cm, which is separated into two equal parts of 3 cm × 5 cm × 1.5 cm by a Nafion 115 membrane (DuPont, Wilmington, DE). The electrolytes were stored in two external reservoirs (each 25 mL). The electrolyte was pumped (flow rate of 11.5 cm min⁻¹) through the electrode where the electrochemical reactions occurred. The electrodes were immersed in solution to a depth of 2 cm. Porous carbon felt (5 cm in width and 3 mm in thickness, LZC Works, China) thermally treated at 723 K for 16 h was used as a positive electrode. A titanium sheet was used as a current collector. A zinc sheet (5 cm in width and 1 mm in thickness) negative electrode was polished and washed with water before experiments. Coulombic and energy efficiencies of the zinc–cerium redox flow cell using mixed-acid electrolyte are both higher than those using single CH₃SO₃H electrolyte. As shown in Fig. 2, the time taken for charging the cell using 2.5 mol L⁻¹ CH₃SO₃H as positive supporting electrolyte media is 19 min, corresponding to 65.6% extent of charge. It is 21 min for 3 mol L⁻¹ CH₃SO₃H, corresponding to 72.5% extent of charge. For mixed acid containing 2 mol L⁻¹ CH₃SO₃H and 0.5 mol L⁻¹ H₂SO₄, it is 22.5 min, reaching a 77.7% extent of charge. High extent of charge indicates high utilization rate of the electrolyte. It helps to improve the practical capacity of the cell. In addition, from this plot, the coulombic and voltage efficiency values are calculated as 85.1% and 80.3% for (a) 2.5 mol L⁻¹ CH₃SO₃H, 85.7% and 84.1% for (b) 3 mol L⁻¹ CH₃SO₃H, 86.7%, and 84.5% for (c) 2 mol L⁻¹ CH₃SO₃H + 0.5 mol L⁻¹ H₂SO₄, respectively.

2.1.3. Additives

In order to further improve the stability of the electrolyte and/or the kinetics of the half-cell reaction, some additives in electrolyte are studied. We have systematically investigated the effect of various additives, such as sulfosalicylic acid (SSA), ethylenediaminetetraacetic acid (EDTA), diethylenetriaminepentaacetate

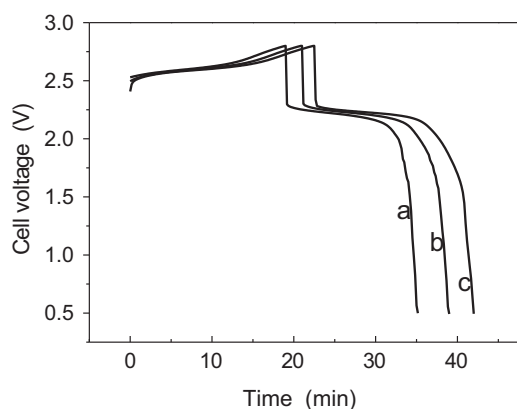


Fig. 2. The typical charge–discharge curves of the Zn/Ce cell using different supporting electrolytes at 293 K [85]. Positive electrolyte (18 mL): 0.3 mol L⁻¹ Ce³⁺ in the following acid solutions, (a) 2.5 mol L⁻¹ MSA; (b) 3 mol L⁻¹ MSA; (c) 2 mol L⁻¹ MSA + 0.5 mol L⁻¹ H₂SO₄. Negative electrolyte (18 mL): 0.3 mol L⁻¹ ZnSO₄ solution.

Table 10Effect of various additives on Ce³⁺/Ce⁴⁺ electrolyte stability and kinetics of Ce³⁺/Ce⁴⁺ electrode reaction.

| Additives | Kinetics | Stability |
|---------------------|-----------------|-----------------|
| Sulfosalicylic acid | Positive effect | Positive effect |
| EDTA | Positive effect | Positive effect |
| DTPA | Positive effect | Positive effect |
| Phthalic anhydride | Positive effect | Positive effect |
| Sulfocarbamide | No effect | Positive effect |
| Carbamide | Negative effect | No effect |
| Sodium citrate | Negative effect | No effect |
| Sodium tetraborate | Negative effect | No effect |
| Silver nitrate | Positive effect | Negative effect |
| Lead acetate | Negative effect | Negative effect |
| Cobalt acetate | Positive effect | No effect |

(DTPA), phthalic anhydride, sulfocarbamide, carbamide, sodium citrate, sodium tetraborate, silver nitrate, lead acetate and cobalt acetate, on kinetics of Ce³⁺/Ce⁴⁺ electrode reaction and stability of Ce³⁺/Ce⁴⁺ electrolyte [86,110]. Interestingly, as shown in Table 10, when sulfosalicylic acid, EDTA, DTPA and phthalic anhydride are added into the cerium electrolyte, both the kinetics of the Ce³⁺/Ce⁴⁺ electrode reaction and stability of Ce³⁺/Ce⁴⁺ electrolyte are improved. On the other hand, sulfocarbamide has positive effect on the stability of the Ce³⁺/Ce⁴⁺ electrolyte and no effect on the kinetics of the Ce³⁺/Ce⁴⁺ electrode reaction, while silver nitrate has positive effect on the kinetics of the Ce³⁺/Ce⁴⁺ electrode reaction and negative effect on the stability of the Ce³⁺/Ce⁴⁺ electrolyte.

As shown in Fig. 3, the cathodic and anodic peaks for the Ce³⁺/Ce⁴⁺ redox couple are located between 1.2 and 1.4 V vs. SCE. At this potential range, the distinct anodic peak could not be observed for the oxidation of sulfosalicylic acid. Furthermore, the voltammetry of sulfosalicylic acid lacks the return peak. Hence, the increase in peak current for Ce³⁺/Ce⁴⁺ redox couple in the presence

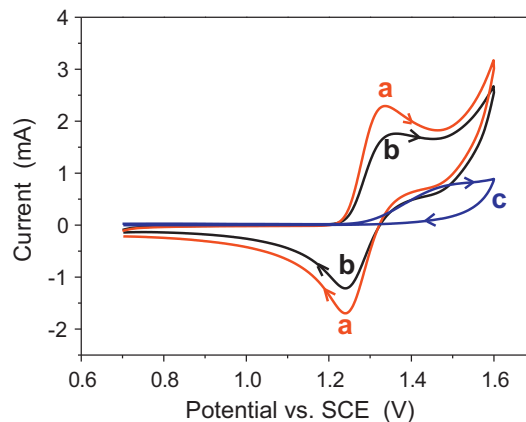


Fig. 3. Effect of SSA on cyclic voltammogram for Ce³⁺/Ce⁴⁺ redox couple. Concentration: [Ce³⁺] = [Ce⁴⁺] = 5 mmol L⁻¹, [SSA] = 0.5 mmol L⁻¹, [H₂SO₄] = 1 mol L⁻¹. (a) in the presence of SSA; (b) in the absence of SSA; (c) for 0.5 mmol L⁻¹ SSA in 1 mol L⁻¹ H₂SO₄ solution without cerium. Scan rate: 10 mV s⁻¹. SSA, sulfosalicylic acid.

Table 11
Effect of sulfosalicylic acid(SA) on stability of $\text{Ce}^{3+}/\text{Ce}^{4+}$ electrolyte.

| SA (mmol L ⁻¹) | MA (mol L ⁻¹) | Ce^{3+} (mol L ⁻¹) | Temperature (K) | State of charge (%) | | | |
|----------------------------|---------------------------|---|-----------------|---------------------|---------|---------|---------|
| | | | | 50 | 70 | 90 | 100 |
| 0 | 3 | 1 | 293 | 30 days | 30 days | 30 days | 30 days |
| 0.5 | 3 | 1 | 293 | 30 days | 30 days | 30 days | 30 days |
| 0 | 3 | 1 | 313 | 30 days | 30 days | 30 days | 30 days |
| 0.5 | 3 | 1 | 313 | 30 days | 30 days | 30 days | 30 days |
| 0 | 3 | 1 | 333 | 30 days | 30 days | 30 days | 30 days |
| 0.5 | 3 | 1 | 333 | 30 days | 30 days | 30 days | 30 days |
| 0 | 1 | 1 | 293 | 30 days | 30 days | 30 days | 30 days |
| 0.5 | 1 | 1 | 293 | 30 days | 30 days | 30 days | 30 days |
| 0 | 1 | 1 | 313 | 30 days | 30 days | 30 days | 30 days |
| 0.5 | 1 | 1 | 313 | 30 days | 30 days | 30 days | 30 days |
| 0 | 1 | 1 | 333 | 30 days | 30 days | 30 days | 12 days |
| 0.5 | 1 | 1 | 333 | 30 days | 30 days | 30 days | 20 days |
| 0 | 1 | 2 | 293 | 30 days | – | – | – |
| 0.5 | 1 | 2 | 293 | 30 days | – | – | – |
| 0 | 1 | 2 | 313 | 30 days | – | – | – |
| 0.5 | 1 | 2 | 313 | 30 days | – | – | – |
| 0 | 1 | 2 | 333 | 18 days | – | – | – |
| 0.5 | 1 | 2 | 333 | 25 days | – | – | – |

Note. Day number in the table means no precipitation in this period.

of sulfosalicylic acid is not caused by the oxidation and reduction of sulfosalicylic acid, but due to the improvement of kinetics of the $\text{Ce}^{3+}/\text{Ce}^{4+}$ redox couple by sulfosalicylic acid. The diffusion coefficient of Ce^{3+} is $6.5 \times 10^{-6} \text{ cm}^2 \text{ s}^{-1}$ and the standard rate constant of the $\text{Ce}^{3+}/\text{Ce}^{4+}$ redox reaction is $3.2 \times 10^{-4} \text{ cm s}^{-1}$ in the presence of sulfosalicylic acid, which are all larger than those in the absence of sulfosalicylic acid ($3.6 \times 10^{-6} \text{ cm}^2 \text{ s}^{-1}$, $2.0 \times 10^{-4} \text{ cm s}^{-1}$) [110]. The explanation is not given about the change of diffusion coefficient and the standard rate constant in the literature. Generally, the diffusion coefficient of the $\text{Ce}^{3+}/\text{Ce}^{4+}$ should decrease with the increase of component in the electrolyte. The above result is not consistent with the expectation, which needs further study. As shown in Table 11, precipitation can be found after 12 days in a solution containing $1 \text{ mol L}^{-1} \text{ Ce}^{3+}$ and $1 \text{ mol L}^{-1} \text{ CH}_3\text{SO}_3\text{H}$ at 100% state of charge at 333 K; whereas it took 20 days for precipitation appearing in a solution containing 0.5 mmol L^{-1} sulfosalicylic acid, $1 \text{ mol L}^{-1} \text{ Ce}^{3+}$ and $1 \text{ mol L}^{-1} \text{ CH}_3\text{SO}_3\text{H}$ at 100% state of charge at 333 K. So addition of sulfosalicylic acid can lead to the improvement of $\text{Ce}^{3+}/\text{Ce}^{4+}$ electrolyte stability.

2.1.4. Mixed electrolyte

Theoretically, to increase the special energy of ZCB, concentration of the active materials in the electrolyte should be further increased. To this end, compared with above-mentioned electrolyte systems such as single acid medium and mixed acid medium with or without additives, mixed electrolyte seems to be more powerful. Mixed electrolyte means that an electrolyte contains no less than two redox couples. Up to now, two kinds of mixed electrolyte have been investigated: [86] cerium & Nitroso-R-salt (NRS, 1-Nitroso-2-naphthol-3,6- disuphonic acid disodium) and cerium & ferrum. In a zinc cerium & NRS redox flow cell, $\text{Ce}^{3+}/\text{Ce}^{4+}$ & NRS mixed electrolyte is used as positive electrolyte. In alkaline solution, the electrode reaction of NRS [47] exhibits sluggish electrode kinetics. On the contrary, with rising acid concentration, it exhibits faster electrode kinetics and a diffusion-controlled process. As shown in Fig. 4, with the increase of pH, the peak potential difference increases and the peak current is significantly reduced. When the pH of solutions reaches 14, a weak oxidation peak appears on the voltammogram without the corresponding reduction peak. This indicates that the oxidation product of NRS is difficult to be reduced in strongly alkaline solutions of pH up to 14. In acidic solution of pH 0, NRS is favorable for the application of NRS in redox flow battery.

In a zinc cerium & ferrum redox flow cell, positive electrolyte is a solution containing $\text{Ce}^{3+}/\text{Ce}^{4+}$ & $\text{Fe}^{2+}/\text{Fe}^{3+}$ couples. Kinetics of $\text{Fe}^{2+}/\text{Fe}^{3+}$ electrode process is faster than that of $\text{Ce}^{3+}/\text{Ce}^{4+}$ electrode process. The exchange current density is $3.92 \times 10^{-3} \text{ A cm}^{-2}$ for $\text{Fe}^{2+}/\text{Fe}^{3+}$ electrode process on platinum [86], which is larger than that of $\text{Ce}^{3+}/\text{Ce}^{4+}$. The diffusion coefficient is $6.62 \times 10^{-6} \text{ cm}^2 \text{ s}^{-1}$ for Fe^{2+} ion; $3.62 \times 10^{-6} \text{ cm}^2 \text{ s}^{-1}$ for Fe^{3+} ion. Charge–discharge capacities of zinc–cerium & nitroso cell as well as zinc–cerium & ferrum redox flow cell are larger than that of zinc–cerium redox flow cell. Performance of zinc–cerium & ferrum redox flow cell is better than that of zinc–cerium & nitroso redox flow cell at large charge–discharge current. As shown in Fig. 5, using mixed electrolyte as positive electrolyte, there appears two charge platforms and two discharge platforms. Platform *a* corresponds to the oxidation process of NRS, *b* to the oxidation process of Ce^{3+} ion, *c* to the reduction process of Ce^{4+} ion, *d* to the reduction process of the product from the NRS oxidation process. However, there is only one charge platform and one discharge platform for zinc–cerium redox cell.

2.2. Electrode

Normally, in a redox flow battery system, inert material is used as electrode. An ideal electrode should possess

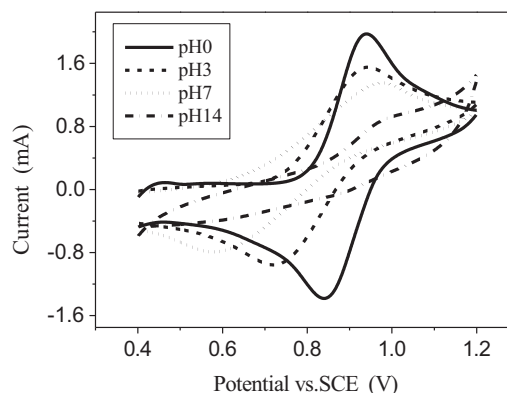


Fig. 4. Influence of pH on the cyclic voltammograms for 50 mmol L^{-1} NRS solution at a platinum electrode. NRS, 1-Nitroso-2-naphthol-3,6-disuphonic acid disodium.

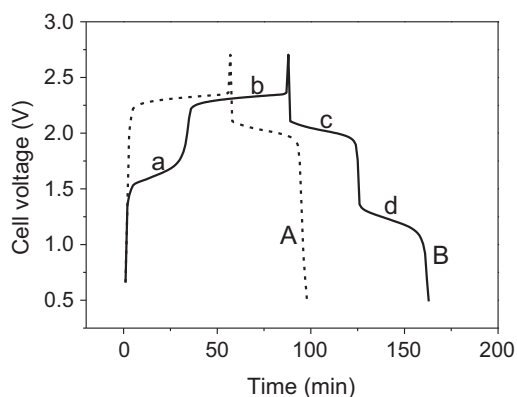


Fig. 5. Performance of zinc-cerium & NRS redox flow cell. Positive electrolyte: (A) $0.1 \text{ mol L}^{-1} \text{ Ce}(\text{CH}_3\text{SO}_3)_3 + 1 \text{ mol L}^{-1} \text{ CH}_3\text{SO}_3\text{H} + 0.5 \text{ mol L}^{-1} \text{ H}_2\text{SO}_4$; (B) $0.1 \text{ mol L}^{-1} \text{ Ce}(\text{CH}_3\text{SO}_3)_3 + 0.025 \text{ mol L}^{-1} \text{ NRS} + 1 \text{ mol L}^{-1} \text{ CH}_3\text{SO}_3\text{H} + 0.5 \text{ mol L}^{-1} \text{ H}_2\text{SO}_4$. NRS, 1-Nitroso-2-naphthol-3,6-disulphonic acid disodium. (a) charging platform corresponding to NRS, (b) charging platform corresponding to Ce^{3+} , (c) discharging platform corresponding to Ce^{4+} , (d) discharging platform corresponding to the oxidized NRS.

high electric conductivity and long cyclic life in acid solution containing concentrated and oxidizing tetravalent cerium ion (Ce^{4+}). The electrochemical behaviors of $\text{Ce}^{3+}/\text{Ce}^{4+}$ on different electrodes such as gold [92,96,99], diamond [98], graphite [81,85,100], platinum [82,84,85,91,97,99–101,110], glassy carbon [95,99,100,102,103,105–107], carbon felt [83,108] have been investigated. As illustrated in Table 12, k_0 values are reported to be between 2.0×10^{-6} and $4.0 \times 10^{-2} \text{ cm s}^{-1}$. It is well known that electrochemical reactions are heterogeneous in nature with the reaction kinetics controlled by the properties of the electrode–electrolyte interface and the concentration of reactant available at this interface. Hence, the physical, chemical, and electronic properties of the electrode surface are of critical importance. Besides the type of electrode, the surface chemistry of electrode significantly affects the electrochemical performance of the electrode. To this end, the pretreatment of the electrode is crucial and is electrode materials-dependent.

To compare the kinetic parameters for $\text{Ce}^{3+}/\text{Ce}^{4+}$ system at Platinum and graphite electrode, a model electrolyte containing 2 mol L^{-1} methanesulfonic acid, 0.25 mol L^{-1} each of Ce^{3+} and Ce^{4+} is employed. Prior to test, in order to make it ready for the electrochemical measurement, the electrodes are pretreated as follows: [81] after ground with emery paper 1000 grade, the graphite electrode is washed by ultrasonic cleaning in doubly distilled water for ten minutes; the platinum electrodes are cycled in 1 mol L^{-1} sulfuric acid solution between -0.3 and 1.8 V vs. SCE for 25 min at a scan rate of 15 mV s^{-1} . As listed in Table 12, it is found that the $\text{Ce}^{3+}/\text{Ce}^{4+}$ redox reaction exhibits a faster kinetics at graphite

Table 12
Kinetic parameters for $\text{Ce}^{3+}/\text{Ce}^{4+}$ system at different electrodes.

| Electrode | Exchange current density (mA cm^{-2}) | Standard rate constants (10^4 cm s^{-1}) |
|---------------------------------|--|--|
| Platinum [81] | 1.32 | 0.55 |
| Graphite [81] | 9.8 | 4.06 |
| Gold [96] | – | 1.8–2.1 |
| Iridium [96] | – | 3.2–4.3 |
| Glassy carbon [96] | – | 2.4–3.2 |
| Platinum [97] | – | 0.035–0.121 |
| Highly boron-doped diamond [98] | 0.0019–0.015 | 0.02–0.16 |
| Platinum [100] | – | 2.18–4.1 |
| Platinum [101] | – | 1.6–3.1 |
| Glassy carbon [105] | – | 20–260 |
| Glassy carbon [106] | – | 330 ± 70 |

electrode than at platinum electrode. In detail, the exchange current density is calculated to be 1.32 mA cm^{-2} at platinum electrode [81], whereas it is 9.8 mA cm^{-2} at graphite electrode [81]. Kiekens et al. [96] studied and compared the electrochemical performances of gold, iridium and glassy carbon electrode, wherein a standard metallographic procedures are employed for polishing the gold, iridium and glassy carbon electrodes; finally polished with 0.05μ alumina on Buehler microcloth to a mirrorlike finish; then rinsed with water and electrochemically pretreated in separate vessels containing $1 \text{ mol L}^{-1} \text{ H}_2\text{SO}_4$. The gold electrode is oxidized at 1.5 V vs. SCE for 3 min, followed by reduction at -0.3 V vs. SCE for the same time; then the potential is cycled between 1.5 and -0.3 V vs. SCE at a scan rate of 100 mV s^{-1} until reproducible curves are obtained. A same pretreatment is used for the iridium electrode between 1.3 and -0.15 V vs. SCE. The glassy carbon electrode is cycled between 1.3 and -1.0 V vs. SCE for ten minutes at a scan rate of 30 mV s^{-1} after which it is held successively at -0.5 and 0 V vs. SCE for 5 min. Nitrogen is passed through the solution during the pretreatment. As shown in Table 12, the standard rate constant for $\text{Ce}^{3+}/\text{Ce}^{4+}$ system in $1 \text{ mol L}^{-1} \text{ H}_2\text{SO}_4$ is $3.2\text{--}4.3 \times 10^{-4} \text{ cm s}^{-1}$ at iridium electrode, $2.4\text{--}3.2 \times 10^{-4} \text{ cm s}^{-1}$ at glassy carbon electrode, $1.8\text{--}2.1 \times 10^{-4} \text{ cm s}^{-1}$ at gold electrode, indicating that iridium electrode has the best activation.

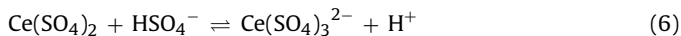
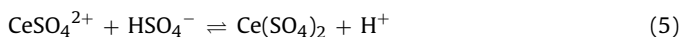
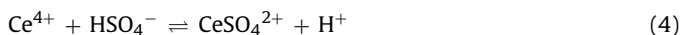
Randle and Kuhn [97] reported the oxidation and reduction kinetics of the $\text{Ce}^{3+}/\text{Ce}^{4+}$ redox reaction at a Pt electrode in sulphuric acid. In contrast to previously reported studies, the thickness of platinum oxide on the electrode surface was standardized. The pretreatment of electrode is as following: the platinum electrode is chemically cleaned initially ($\text{H}_2\text{SO}_4/\text{HNO}_3$) and subsequently, at the commencement of each experimental session, by potential cycling between 1.800 and -0.600 V vs. Hg/HgSO_4 for 20 min at 50 mV s^{-1} . Adsorption of Ce^{3+} on oxidized platinum reached a maximum at 1.6 V vs. NHE [97]. At high overpotentials the reduction reaction is first order in Ce^{4+} . Oxidation current at any potential continues to increase with decreasing pH. The half-wave potentials are independent of pH below 1.32, indicating a zero-order dependence on H^+ .

Liu et al. [100] pretreated the platinum electrode using a ten minutes ultrasonication followed by potential cycling for 20 min at 50 mV s^{-1} between 1.80 and -0.6 V vs. Hg/HgSO_4 electrode, then a potential program is used to record polarization curves for producing a layer of constant platinum oxide thickness. The glassy carbon electrode is cycled between 1.3 and -1.0 V vs. SCE for 10 min at a scan rate of 30 mV s^{-1} after which it is held successively at 0.5 and 0 V vs. SCE for 5 min. By the above pretreatment, the type I platinum oxide would reach an apparently limiting covered thickness. Type I platinum oxide existed in the form of PtO_2 , is a good electronic conductor; its conductivity is the same as platinum metal. Judged by the peak potentials difference, the reversibility of the $\text{Ce}^{3+}/\text{Ce}^{4+}$ couple at the graphite electrode is the best, then the glassy carbon electrode, and the platinum electrode is the poorest. Because of no adsorption of Ce^{3+} or Ce^{4+} and formation of oxides on the surface of glassy carbon and graphite electrodes, these carbon electrodes are more suitable for the $\text{Ce}^{3+}/\text{Ce}^{4+}$ system than a platinum electrode.

In addition, eight two and three-dimensional electrodes ($7 \text{ cm} \times 5 \text{ cm} \times 0.2 \text{ cm}$ platinized titanium, $7 \text{ cm} \times 5 \text{ cm} \times 0.6 \text{ cm}$ graphite, $7 \text{ cm} \times 5 \text{ cm} \times 0.6 \text{ cm}$ carbon-polyvinylester, $4.5 \text{ cm} \times 2 \text{ cm} \times 2 \text{ cm}$ 30 ppi reticulated vitreous carbon, $4.5 \text{ cm} \times 2 \text{ cm} \times 2 \text{ cm}$ 100 ppi reticulated vitreous carbon, $4.5 \text{ cm} \times 2 \text{ cm} \times 0.8 \text{ cm}$ Alfa Aesar carbon felt, $4.5 \text{ cm} \times 2 \text{ cm} \times 0.8 \text{ cm}$ Sigratherm[®] carbon felt, four $4.4 \text{ cm} \times 1.6 \text{ cm} \times 0.25 \text{ cm}$ platinized titanium mesh welded on a $7 \text{ cm} \times 5 \text{ cm} \times 0.2 \text{ cm}$ platinized titanium plate) were tested by Leung et al. [83] under both constant current density and constant cell voltage discharge. They found that carbon felt and the three-dimensional platinized titanium mesh electrodes exhibited superior performance over the 2-dimensional electrodes.

3. Reaction mechanism

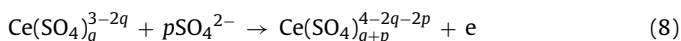
It is crucial to understand the half-cell reaction mechanisms in the acid medium. In sulfuric acid solution [97,100], the Ce^{4+} could form the following complexes with SO_4^{2-} :



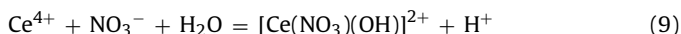
The equilibrium constants are 3500, 200 and 20 for reactions (4)–(6), respectively. The $\text{Ce}^{3+}/\text{Ce}^{4+}$ electrode process is not simply a one-electron transfer reaction:



The possible half-cell reaction may be:



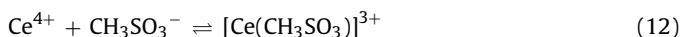
In nitric acid medium [98], the Ce^{4+} could form the following complexes with NO_3^- :



In HClO_4 solution [98], the Ce^{3+} could form the following complexes with H_2O :



The equilibrium constants for reactions (10) and (11) have been reported to be 5.2 and 16.5, respectively. In $\text{CH}_3\text{SO}_3\text{H}$ solution [86,102], the $\text{Ce}^{3+}/\text{Ce}^{4+}$ redox couple can also exist as methanesulfonate complexes (However, the equilibrium constants for 12 and 13 are not given in the literatures):



The possible half-cell reaction may be:

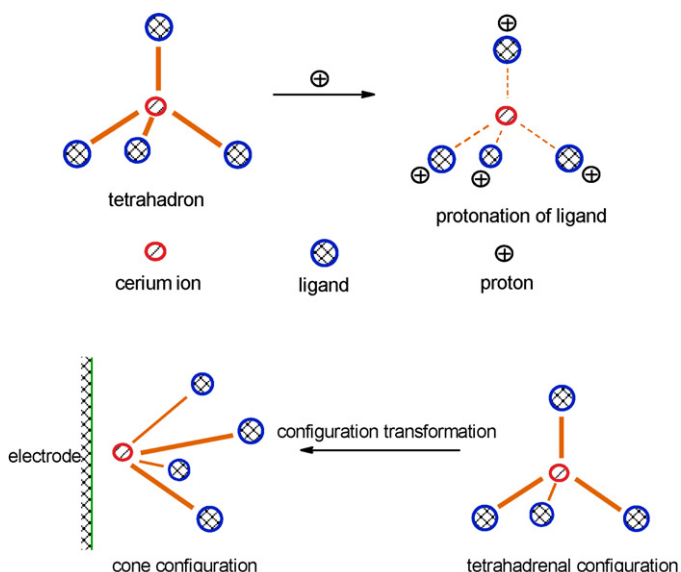
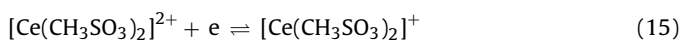


Fig. 6. Protonation and configuration transformation of cerium complex ion.

We have proposed a proton-effect model related to the $\text{Ce}^{3+}/\text{Ce}^{4+}$ electrode process [86]. According to the valence bond theory, complex ion exists in a certain spatial configuration, which can make the system energy reach the lowest point. For example, $[\text{Ag}(\text{NH}_3)_2]^+$, $[\text{AgBr}_2]^-$, $[\text{Cu}(\text{NH}_3)_2]^+$ and $[\text{Ag}(\text{CN})_2]^-$ are linear species; $[\text{HgI}_3]^-$ is triangular species; $[\text{BeF}_4]^{2-}$, $[\text{BF}_4]^-$, $[\text{HgCl}_4]^{2-}$ and $[\text{Zn}(\text{NH}_4)]^{2-}$ are normal tetrahedral configuration. As shown in Fig. 6, it is an assumption that $\text{Ce}^{3+}/\text{Ce}^{4+}$ complex ion has a tetrahedral configuration. The cerium ion lies in the center of the tetrahedral configuration. The $\text{Ce}^{3+}/\text{Ce}^{4+}$ ions must approach the electrode as possible as they can in order to donate/receive electron; hence, cerium complex ion experiences a configuration transformation before the $\text{Ce}^{3+}/\text{Ce}^{4+}$ charge transfer process. After configuration transformation, the position of the cerium ion changed from the center of the normal tetrahedron to the top of the cone. The active energy of configuration transformation is proportional to bond energy of coordinating bond. Protonation of ligand can weaken the coordinating bond and thus higher proton concentration would benefit the charge transfer process.

4. Conclusions and perspective

This review first summarizes the methods to improve the kinetics of cerium half-cell and/or the cell capacity: (i) using the single acid medium, in which the cerium salt has a good solubility, (ii) using mixed acid, (iii) using additives, and (iv) using mixed electrolyte. These methods, especially the idea, will benefit the improvement of other redox flow battery, even many other batteries.

Zinc–cerium redox flow batteries have received increasing attention as possible batteries for energy storage applications. Although significant developments have been achieved, the ZCB is still at an embryo stage and there are numerous scientific and technical challenges that must be overcome. From the viewpoint of the authors, the key areas for future research are as follows:

- (1) The evolution of oxygen in cerium half-cell during charging process. The oxidation of Ce^{3+} to Ce^{4+} takes place at a very positive potential range (1.2–1.7 V vs. NHE). Hence, the evolution of oxygen during charging is a noticeable vice-reaction.
- (2) Design and synthesis of positive electrode material with high chemical stability in the electrolyte containing strong acid medium and oxidized Ce^{4+} . The life time of ZCB is significantly affected by the chemical stability of positive electrode material. The $\text{Ce}^{3+}/\text{Ce}^{4+}$ electrolyte has strong oxidisability, which makes the chemical stability of positive electrode material become a most important requirement in ZCB system.
- (3) Zinc deposition on negative electrode in acid medium. To this day, there is no detailed report about the investigation of zinc deposition in acid medium.

In addition, it is necessary for understanding of the complex chemical reaction mechanisms that occur during charge and discharge, including the logistics balance mechanism, electrochemical performance degradation mechanism and stability regulation mechanisms of ZCB in the long term operation.

The scientific and technical impediments facing development of practical ZCB open up an exciting opportunity for researchers with different backgrounds to utilize their unique knowledge and skills to bridge the knowledge gaps that exist in the field of the ZCB.

Acknowledgements

This work is financially supported by 100 Talents Programme of The Chinese Academy of Sciences, Foundation for Innovative

Research Groups of the National Natural Science Foundation of China (Grant No. 20921002), National Natural Science Foundation of China (Grant No. 21101147), and Jiangxi University of Science and Technology (No. jxxj12022).

References

- [1] T.M. Razykov, C.S. Ferekides, D. Morel, E. Stefanakos, H.S. Ullal, H.M. Upadhyaya, Solar photovoltaic electricity: Current status and future prospects, *Solar Energy* 85 (2011) 1580.
- [2] A.M. Foley, P.G. Leahy, A. Marvuglia, E.J. McKeogh, Current methods and advances in forecasting of wind power generation, *Renewable Energy* 37 (2012) 1.
- [3] T. Ackermann, L. Söder, An overview of wind energy-status 2002, *Renewable and Sustainable Energy Reviews* 6 (2002) 67.
- [4] R.M. Dell, D.A.J. Rand, Energy storage – a key technology for global energy sustainability, *Journal of Power Sources* 100 (2001) 2.
- [5] H. Ibrahim, A. Ilinca, J. Perron, Energy storage systems – characteristics and comparisons, *Renewable and Sustainable Energy Reviews* 12 (2008) 1221.
- [6] K.C. Divya, J. Østergaard, Battery energy storage technology for power systems – an overview, *Electric Power Systems Research* 79 (2009) 511.
- [7] F. Beck, P. Rüetschi, Rechargeable batteries with aqueous electrolytes, *Electrochimica Acta* 45 (2000) 2467.
- [8] C. Ponce de León, A. Frías-Ferrer, J. González-García, D.A. Szánto, F.C. Walsh, Redox flow cells for energy conversion, *Journal of Power Sources* 160 (2006) 716.
- [9] C.K. Jia, J.G. Liu, C.W. Yan, A significant improved membrane for vanadium redox flow battery, *Journal of Power Sources* 195 (2010) 4380.
- [10] S.H. Ge, B.L. Yi, H.M. Zhang, Study of a high power density sodium polysulfide/bromine energy storage cell, *Journal of Applied Electrochemistry* 34 (2004) 181.
- [11] Y. Qin, J.G. Liu, Y.Y. Di, C.W. Yan, C.L. Zeng, J.Z. Yang, Thermodynamic investigation of electrolytes of the vanadium redox flow battery (II): A study on low-temperature heat capacities and thermodynamic properties of $\text{VOSO}_4 \cdot 2.63\text{H}_2\text{O}(\text{s})$, *Journal of Chemical and Engineering Data* 55 (2010) 1276.
- [12] G. Oriji, Y. Katayama, T. Miura, Investigation on V(IV)/V(V) species in a vanadium redox flow battery, *Electrochimica Acta* 49 (2004) 3091.
- [13] M. Kazacos, M. Cheng, M. Skyllas-kazacos, Vanadium redox cell electrolyte optimization studies, *Journal of Applied Electrochemistry* 20 (1990) 463.
- [14] F. Rahman, M. Skyllas-Kazacos, Vanadium redox battery: Positive half-cell electrolytes studies, *Journal of Power Sources* 189 (2009) 1212.
- [15] H.Q. Zhu, Y.M. Zhang, L. Yue, W.S. Li, G.L. Li, D. Shu, H.Y. Chen, Graphite-carbon nanotube composite electrode for all vanadium redox flow battery, *Journal of Power Sources* 184 (2008) 637.
- [16] W.H. Wang, X.D. Wang, Investigation of Ir-modified carbon felt as the positive electrode of an all-vanadium redox flow battery, *Electrochimica Acta* 52 (2007) 6755.
- [17] P. Qian, H. Zhang, J. Chen, Y.H. Wen, Q.T. Luo, Z.H. Liu, D.J. You, B.L. Yi, A novel electrode-bipolar plate assembly for vanadium redox flow battery applications, *Journal of Power Sources* 175 (2008) 613.
- [18] X.G. Li, K.L. Huang, S.Q. Liu, N. Tan, L.Q. Chen, Characteristics of graphite felt electrode electrochemically oxidized for vanadium redox battery application, *Transactions of Nonferrous Metals Society of China* 17 (2007) 195.
- [19] L. Yue, W.S. Li, F.Q. Sun, L.Z. Zhao, L.D. Xing, Highly hydroxylated carbon fibres as electrode materials of all-vanadium redox flow battery, *Carbon* 48 (2010) 3079.
- [20] R. Zito Jr., Zinc-bromine battery with long term stability, US Patent 4482614 (1984).
- [21] E. Kantner, Zinc-bromine batteries with improved electrolyte, US Patent 4491625 (1985).
- [22] T. Sasaki, K. Tange, M. Okawa, Zinc-bromine battery, US Patent 4663251 (1987).
- [23] G. Tomazic, Zinc-bromine battery with circulating electrolytes, US Patent 5607788 (1997).
- [24] P.M. Hoobin, K.J. Cathro, Stability of zinc/bromine battery electrolytes, *Journal of Applied Electrochemistry* 19 (1989) 943.
- [25] R.L. Clarke, B. Dougherty, S. Harrison, J.P. Millington, S. Mohanta, Mixed electrolyte battery, US Patent 7560189 B2 (2009).
- [26] R.L. Clarke, B. Dougherty, S. Harrison, J.P. Millington, S. Mohanta, Cerium batteries, US Patent 7625663 B2 (2009).
- [27] R.L. Clarke, B. Dougherty, S. Harrison, J.P. Millington, S. Mohanta, Lanthanide batteries, WO 03/017408 A1 (2003).
- [28] R.L. Clarke, B. Dougherty, S. Harrison, J.P. Millington, S. Mohanta, Load leveling battery and methods therefor, US Patent 2004/0197649 A1 (2004).
- [29] R.L. Clarke, B. Dougherty, S. Harrison, J.P. Millington, S. Mohanta, Battery with gelled electrolyte, US Patent 2008/0233484 A1 (2008).
- [30] X. Li, D. Pletcher, F.C. Walsh, A novel flow battery: A lead acid battery based on an electrolyte with soluble lead(II) Part VII. Further studies of the lead dioxide positive electrode, *Electrochimica Acta* 54 (2009) 688.
- [31] D. Pletcher, H. Zhou, G. Kear, C.T. John Low, F.C. Walsh, R.G.A. Wills, A novel flow battery—A lead-acid battery based on an electrolyte with soluble lead(II) Part VI. Studies of the lead dioxide positive electrode, *Journal of Power Sources* 180 (2008) 630.
- [32] D. Pletcher, H. Zhou, G. Kear, C.T. John Low, F.C. Walsh, R.G.A. Wills, A novel flow battery—A lead-acid battery based on an electrolyte with soluble lead(II) V. Studies of the lead negative electrode, *Journal of Power Sources* 180 (2008) 621.
- [33] H.Y. Peng, H.Y. Chen, W.S. Li, S.J. Li, J.M. Nan, Z.H. Xu, A study on the reversibility of Pb(II)/PbO₂ conversion for the application of flow liquid battery, *Journal of Power Sources* 168 (2007) 105.
- [34] R.G.A. Wills, J. Collins, D. Stratton-Campbell, C.T.J. Low, D. Pletcher, F.C. Walsh, Developments in the soluble lead-acid flow battery, *Journal of Applied Electrochemistry* 40 (2009) 955.
- [35] A. Oury, A. Kirchev, Y. Bultel, E. Chainet, PbO₂/Pb²⁺ cycling in methanesulfonic acid and mechanisms associated for soluble lead-acid flow battery applications, *Electrochimica Acta* 71 (2012) 140.
- [36] A.A. Shinkle, A.E.S. Sleightholme, L.D. Griffith, L.T. Thompson, C.W. Monroe, Degradation mechanisms in the non-aqueous vanadium acetylacetonate redox flow battery, *Journal of Power Sources* 206 (2011) 490.
- [37] C.H. Bae, E.P.L. Roberts, R.A.W. Dryfe, Chromium redox couples for application to redox flow batteries, *Electrochimica Acta* 48 (2002) 279.
- [38] Q.H. Liu, A.A. Shinkle, Y.D. Li, C.W. Monroe, L.T. Thompson, A.E.S. Sleightholme, Non-aqueous chromium acetylacetonate electrolyte for redox flow batteries, *Electrochimica Acta* 51 (2006) 1634.
- [39] A.E.S. Sleightholme, A.A. Shinkle, Q.H. Liu, Y.D. Li, C.W. Monroe, L.T. Thompson, Non-aqueous manganese acetylacetonate electrolyte for redox flow batteries, *Journal of Power Sources* 196 (2011) 5742.
- [40] M.H. Chakrabarti, R.A.W. Dryfe, E.P.L. Roberts, Evaluation of electrolytes for redox flow battery applications, *Electrochimica Acta* 52 (2007) 2189.
- [41] M. Skyllas-Kazacos, Novel vanadium chloride/polyhalide redox flow battery, *Journal of Power Sources* 124 (2003) 299.
- [42] Y.H. Wen, H.M. Zhang, P. Qian, H.T. Zhou, P. Zhao, B.L. Yi, Y.S. Yang, A study of the Fe(III)/Fe(II)-triethanolamine complex redox couple for redox flow battery application, *Electrochimica Acta* 51 (2006) 3769.
- [43] M. Keshavarz, A. Varadarajan, Methods for the preparation of electrolytes for chromium-iron redox flow batteries, US Patent 2010/0261070 A1 (2010).
- [44] P.S. Fedkiw, R.W. Watts, A mathematical model for the iron/chromium redox battery, *Journal of the Electrochemical Society* 131 (1984) 701.
- [45] B. Fang, S. Iwasa, Y. Wei, T. Arai, M. Kumagai, A study of the Ce(III)/Ce(IV) redox couple for redox flow battery application, *Electrochimica Acta* 47 (2002) 3971.
- [46] Y. Xu, Y.H. Wen, J. Cheng, G.P. Cao, Y.S. Yang, A study of tiron in aqueous solutions for redox flow battery application, *Electrochimica Acta* 55 (2010) 715.
- [47] Z.P. Xie, F.J. Xiong, D.B. Zhou, Nitroso-R-salt in aqueous solutions for redox flow battery application, *Advanced Materials Research* 239–242 (2011) 2813.
- [48] Y. Xu, Y.H. Wen, J. Cheng, G.P. Cao, Y.S. Yang, Study on a single flow acid Cd-chloranil battery, *Electrochemistry Communications* 11 (2009) 1422.
- [49] J.Q. Pan, Y.Z. Sun, J. Cheng, Y.H. Wen, Y.S. Yang, P.Y. Wan, Study on a new single flow acid Cu-PbO₂ battery, *Electrochemistry Communications* 10 (2008) 1226.
- [50] Q.H. Wang, L.F. Jiao, H.M. Du, Q.N. Huan, W.X. Peng, D.W. Song, Y.J. Wang, H.T. Yuan, Investigation of novel cobalt-boron-carbon system as negative material for secondary alkaline battery, *Electrochimica Acta* 58 (2011) 437.
- [51] M.P.S. Krekeler, H.A. Barrett, R. Davis, C. Burnette, T. Doran, A. Ferraro, A. Meyer, An investigation of mass and brand diversity in a spent battery recycling collection with an emphasis on spent alkaline batteries: Implications for waste management and future policy concerns, *Journal of Power Sources* 203 (2012) 222.
- [52] X.W. Yu, S. Licht, High capacity alkaline super-iron boride battery, *Electrochimica Acta* 52 (2007) 8138.
- [53] C.Y. Kao, Y.R. Tsai, K.S. Chou, Synthesis and characterization of the iron/copper composite as an electrode material for the rechargeable alkaline battery, *Journal of Power Sources* 196 (2011) 5746.
- [54] T.T. Yang, L. Cai, R.E. White, Mathematical modeling of the LiAl/FeS₂ high temperature battery system, *Journal of Power Sources* 201 (2012) 322.
- [55] Q.C. Hu, S. Osswald, R. Daniel, Y. Zhu, S. Wesel, L. Ortiz, D.R. Sadoway, Graft copolymer-based lithium-ion battery for high-temperature operation, *Journal of Power Sources* 196 (2011) 5604.
- [56] H. Ryu, T. Kim, K. Kim, J.H. Ahn, T. Nam, G.X. Wang, H.J. Ahn, Discharge reaction mechanism of room-temperature sodium-sulfur battery with tetra ethylene glycol dimethyl ether liquid electrolyte, *Journal of Power Sources* 196 (2011) 5186.
- [57] B.K. Purushothaman, J.S. Wainright, Analysis of pressure variations in a low-pressure nickel-hydrogen battery. Part 2: Cells with metal hydride storage, *Journal of Power Sources* 206 (2012) 421.
- [58] B.K. Purushothaman, J.S. Wainright, Analysis of pressure variations in a low-pressure nickel-hydrogen battery: Part 1, *Journal of Power Sources* 206 (2012) 429.
- [59] K.H. Norian, Equivalent circuit components of nickel-cadmium battery at different states of charge, *Journal of Power Sources* 196 (2011) 5205.
- [60] P. Gao, Y. Wang, Q. Zhang, Y.J. Chen, D. Bao, L.Q. Wang, Y.Z. Sun, G.B. Li, M.L. Zhang, Cadmium hydroxide nanowires—new high capacity Ni-Cd battery anode materials without memory effect, *Journal of Materials Chemistry* 22 (2012) 13922.
- [61] K.Z. Fang, D.B. Mu, S. Chen, F. Wu, X.J. Zeng, Thermal behavior of nickel-metal hydride battery during charging at a wide range of ambient temperatures, *Journal of Thermal Analysis and Calorimetry* 105 (2011) 383.

- [62] W.R. Osório, D.M. Rosa, A. Garcia, Electrolyte features and microstructure affecting the electrochemical performance of a Pb-Sb alloy for lead-acid battery components, *Electrochimica Acta* 56 (2011) 8457.
- [63] W.R. Osório, D.M. Rosa, L.C. Peixoto, A. Garcia, Cell/dendrite transition and electrochemical corrosion of Pb-Sb alloys for lead-acid battery applications, *Journal of Power Sources* 196 (2011) 6567.
- [64] C. Soundarrajan, A. Sivasankar, S. Maruthamuthu, A. Veluchamy, Improve lead recovery and sulphate removal from used lead acid battery through electrokinetic technique, *Journal of Hazardous Materials* 217–218 (2012) 452.
- [65] D. Pavlov, G. Petkova, M. Dimitrov, M. Shiomi, M. Tsubota, Influence of fast charge on the life cycle of positive lead-acid battery plates, *Journal of Power Sources* 87 (2000) 39.
- [66] J.E. Manders, N. Bui, D.W.H. Lambert, J. Navarette, R.F. Nelson, E.M. Valeriote, Lead/acid battery design and operation, *Journal of Power Sources* 73 (1998) 152.
- [67] D.W.H. Lambert, J.E. Manders, R.F. Nelson, K. Peters, D.A.J. Rand, M. Stevenson, Strategies for enhancing lead-acid battery production and performance, *Journal of Power Sources* 88 (2000) 130.
- [68] P.T. Moseley, Improving the valve-regulated lead-acid battery, *Journal of Power Sources* 88 (2000) 71.
- [69] K. Micka, Contemporary trends in research and development of lead-acid batteries, *Journal of Solid State Electrochemistry* 8 (2004) 932.
- [70] C.D. Parker, Lead-acid battery energy-storage systems for electricity supply networks, *Journal of Power Sources* 100 (2001) 18.
- [71] M.L. Gopikanth, S. Sathyanarayana, Impedance parameters and the state-of-charge. II. Lead-acid battery, *Journal of Applied Electrochemistry* 9 (1979) 369.
- [72] J.K. Whear, E.H. Miller, M.R. Roberts, Lead acid battery separators, batteries and related methods, US Patent 2012/0070747 A1 (2012).
- [73] P. Isken, C. Dippel, R. Schitz, R.W. Schmitz, M. Kunze, S. Passerini, M. Winter, A. Lex-Balducci, High flash point electrolyte for use in lithium-ion batteries, *Electrochimica Acta* 56 (2011) 7530.
- [74] K. Tasaki, A. Goldberg, M. Winter, On the difference in cycling behaviors of lithium-ion battery cell between the ethylene carbonate- and propylene carbonate-based electrolytes, *Electrochimica Acta* 56 (2011) 10424.
- [75] W.J. Zhang, A review of the electrochemical performance of alloy anodes for lithium-ion batteries, *Journal of Power Sources* 196 (2011) 13.
- [76] X.Y. Wang, X.F. Zhou, K. Yao, J.G. Zhang, Z.P. Liu, A SnO₂/graphene composite as high stability electrode for lithium ion batteries, *Carbon* 49 (2011) 133.
- [77] S. Brutti, J. Hassoun, B. Scrosati, C.Y. Lin, H. Wu, H.W. Hsieh, A high power Sn-C/C-LiFePO₄ lithium ion battery, *Journal of Power Sources* 217 (2012) 72.
- [78] J. Hassoun, D.J. Lee, Y.K. Sun, B. Scrosati, A lithium ion battery using nanostructured Sn-C anode, LiFePO₄ cathode and polyethylene oxide-based electrolyte, *Solid State Ionics* 202 (2011) 36.
- [79] D. Endo, T. Inamasu, T. Nukuda, Y. Katayama, Active material for lithium ion battery having Mg-containing lithium titanate and lithium ion battery, US Patent 8053115 B2 (2011).
- [80] I.C. Halalay, T.J. Fuller, L.J. Zou, S.J. Harris, Lithium ion battery, US Patent 2011/0165459 A1 (2011).
- [81] Z.P. Xie, D.B. Zhou, F.J. Xiong, S.M. Zhang, K.L. Huang, Cerium-zinc redox flow battery: Positive half-cell electrolyte studies, *Journal of Rare Earths* 29 (2011) 567.
- [82] P.K. Leung, C. Ponce de León, C.T.J. Low, Ce(III)/Ce(IV) in methanesulfonic acid as the positive half cell of a redox flow battery, *Electrochimica Acta* 56 (2011) 2145.
- [83] P.K. Leung, C. Ponce de León, C.T.J. Low, A.A. Shah, F.C. Walsh, Characterization of a zinc-cerium flow battery, *Journal of Power Sources* 196 (2011) 5174.
- [84] F.J. Xiong, D.B. Zhou, Z.P. Xie, Y.Y. Chen, A study of the Ce³⁺/Ce⁴⁺ redox couple in sulfamic acid for redox battery application, *Applied Energy*, in press.
- [85] Z.P. Xie, F.J. Xiong, D.B. Zhou, Study of the Ce³⁺/Ce⁴⁺ redox couple in mixed-acid media (CH₃SO₃H and H₂SO₄) for redox flow battery application, *Energy and Fuels* 25 (2011) 2399.
- [86] Z.P. Xie, PhD Thesis, Study of positive electrolyte for zinc-cerium redox flow battery application, Central South University (2011).
- [87] G. Nikiforidis, L. Berlouis, D. Hall, D. Hodgson, Evaluation of carbon composite materials for the negative electrode in the zinc-cerium redox flow cell, *Journal of Power Sources* 206 (2011) 497.
- [88] R.L. Clarke, B.J. Dougherty, S. Harrison, P.J. Millington, S. Mohanta, Cerium Batteries, US Patent 2004/0202925 A1 (2004).
- [89] R.L. Clarke, B.J. Dougherty, S. Harrison, J.P. Millington, S. Mohanta, US Patent 2006/0063065 A1, Battery with bifunctional electrolyte (2005).
- [90] P.K. Leung, C. Ponce-de-León, F.C. Walsh, An undivided zinc-cerium redox flow battery operating at room temperature (295 K), *Electrochemistry Communications* 13 (2011) 770.
- [91] R. Greef, H. Aulich, The kinetics of the cerous-ceric redox reaction at a platinum electrode, *Journal of Electroanalytical Chemistry* 18 (1968) 295.
- [92] R.A. Bonowitz, G.M. Schmid, Oxygen adsorption on gold and the Ce(III)/Ce(IV) reaction, *Journal of the Electrochemical Society* 117 (1970) 1367.
- [93] J.M. Herbelin, T.N. Andersen, H. Eyring, Kinetic parameters by the method of mixed potentials, *Electrochimica Acta* 15 (1970) 1455.
- [94] J.P. Hoare, Effect of dermasorbed oxygen on the catalytic activity of platinum indicator electrodes, *Electrochimica Acta* 17 (1972) 1907.
- [95] R.J. Taylor, A.A. Humffray, Electrochemical studies on glassy carbon electrodes I. Electron transfer kinetics, *Journal of Electroanalytical Chemistry* 42 (1973) 347.
- [96] P. Kiekens, L. Steen, H. Donche, E. Temmerman, Kinetics of Ce(IV) reduction at gold, carbon and iridium electrodes, *Electrochimica Acta* 26 (1981) 841.
- [97] T.H. Randle, A.T. Kuhn, Kinetics and mechanism of the Cerium(IV)/Cerium(III) redox reaction on a platinum electrode, *Journal of the Chemical Society* 79 (1983) 1741.
- [98] Y. Maeda, K. Sato, R. Ramaraj, T.N. Rao, D.A. Tryk, A. Fujishima, The electrochemical response of highly boron-doped conductive diamond electrodes to Ce³⁺ ions in aqueous solution, *Electrochimica Acta* 44 (1999) 3441.
- [99] G.A. Sacchetto, P. Pastore, G. Favaro, M. Fiorani, Liquid chromatographic determination of non-volatile nitrosamines by post-column redox reactions and voltammetric detection at solid electrodes. Behaviour of the Ce(IV)-Ce(III) couple at gold, platinum and glassy carbon electrodes and suitability of the Ce(IV) reagent, *Analytica Chimica Acta* 258 (1992) 99.
- [100] Y. Liu, X. Xia, H. Liu, Studies on cerium (Ce⁴⁺/Ce³⁺)-vanadium(V²⁺/V³⁺) redox flow cell-cyclic voltammogram response of Ce⁴⁺/Ce³⁺ redox couple in H₂SO₄ solution, *Journal of Power Sources* 130 (2004) 299.
- [101] P. Modiba, A.M. Crouch, Electrochemical study of cerium(IV) in the presence of ethylenediaminetetraacetic acid (EDTA) and diethylenetriaminepentaacetate (DTPA) ligands, *Journal of Applied Electrochemistry* 38 (2008) 1293.
- [102] T. Vijayarathai, D. Velayutham, M. Noel, Influence of aromatic reactants and products involved in the two stage electrochemical oxidation on the voltammetric behavior of Ce(IV)/Ce(III) redox couple, *Journal of Applied Electrochemistry* 31 (2001) 979.
- [103] A. Paulenova, S.E. Creager, J.D. Navratil, Y. Wei, Redox potentials and kinetics of the Ce³⁺/Ce⁴⁺ redox reaction and solubility of cerium sulfates in sulfuric acid solutions, *Journal of Power Sources* 109 (2002) 431.
- [104] P. Trinidad, C. Ponce de León, F.C. Walsh, The use of electrolyte redox potential to monitor the Ce(IV)/Ce(III) couple, *Journal of Environment Management* 88 (2008) 1417.
- [105] Y. Wei, B. Fang, T. Arai, M. Kumagai, Electrolytic oxidation of Ce(III) in nitric acid and sulfuric acid media using a flow type cell, *Journal of Applied Electrochemistry* 35 (2005) 561.
- [106] D. Pletcher, E.M. Valdes, Studies of the Ce(III)/Ce(IV) couple in multiphase systems containing a phase transfer reagent-I. conditions for the extraction of Ce(IV) and electrode kinetics, *Electrochimica Acta* 33 (1988) 499.
- [107] T.S. Chen, K.J.C. Yeh, K.L. Huang, Anion effects on the electrochemical regeneration of Ce(IV) in nitric acid used for etching chromium, *Journal of Hazardous Materials* 152 (2008) 922.
- [108] L. Jelínek, Y. Wei, K. Mikio, Electro-oxidation of concentrated Ce(III) at carbon felt anode in nitric acid media, *Journal of Rare Earths* 24 (2006) 257.
- [109] E.G. Jones, F.G. Soper, The nature of the ceric sulphates, *Journal of the Chemical Society* (1935) 802.
- [110] Z.P. Xie, F.J. Xiong, D.B. Zhou, Effect of sulfosalicylic acid on kinetics of Ce³⁺/Ce⁴⁺ electrode reaction, *Advanced Materials Research* 279 (2011) 451.